

Statistical Properties of Thermal Sunyaev-Zel’dovich Maps

Dipak Munshi¹, Shahab Joudaki², Joseph Smidt², Peter Coles¹

¹*School of Physics and Astronomy, Cardiff University, Queen’s Buildings, 5 The Parade, Cardiff, CF24 3AA, UK*

²*Department of Physics and Astronomy, University of California, Irvine, CA 92697*

2 June 2019

ABSTRACT

At high angular frequencies, beyond the damping tail of the primary power spectrum, the dominant contribution to the power spectrum of cosmic microwave background (CMB) temperature fluctuations is the thermal Sunyaev-Zel’dovich (tSZ) effect. We investigate various important statistical properties of the Sunyaev-Zel’dovich maps, using well-motivated models for dark matter clustering to construct statistical descriptions of the tSZ effect to all orders enabling us to determine the entire probability distribution function (PDF). Any generic deterministic biasing scheme can be incorporated in our analysis and the effects of projection, biasing and the underlying density distribution can be analysed separately and transparently in this approach. We introduce the *cumulant correlators* as tools to analyse tSZ catalogs and relate them to corresponding statistical descriptors of the underlying density distribution. The statistics of hot spots in frequency-cleaned tSZ maps are also developed in a self-consistent way to an arbitrary order, to obtain results complementary to those found using the halo model. We also consider different beam sizes, to check the extent to which the PDF can be extracted from various observational configurations. The formalism is presented with two specific models for underlying matter clustering: (1) the hierarchical ansatz; and (2) the lognormal distribution. We find both models to be in very good agreement with the simulation results, though the lognormal model has an edge over the hierarchical model.

Key words: : Cosmology– Sunyaev Zel’dovich Surveys – Methods: analytical, statistical, numerical

1 INTRODUCTION

Measurements of cosmological parameters from Cosmic Microwave Background (CMB) surveys, especially those derived from WMAP¹, have provided cosmologists with a very accurate picture of the background geometry and dynamics of the Universe. However, future all-sky observational programmes with wide frequency coverage - including the ongoing Planck² mission - can open up new possibilities to study secondary effects in the CMB. Indeed, it could be argued that the secondary science that will emerge from Planck is likely to prove even more valuable than the primary science.

Measurements of cosmological parameters from Cosmic Microwave Background (CMB) surveys such as WMAP³ and ongoing Planck⁴ satellite missions can provide a very accurate picture of background geometry and the dynamics of the Universe. However experiments such as Planck with a wide frequency coverage can do so much more. With all-sky coverage and wide range of uncharted frequencies the data provided by experiments such as Planck the secondary science (see e.g. Aghanim, Majumdar, Silk (2008)) can be arguably as valuable as the primary science. In particular, important information concerning the large-scale properties of hot intergalactic gas can be probed using such multifrequency observations. Inverse-Compton scattering of CMB photons - known as the thermal Sunyaev-Zel’dovich effect (tSZ; Sunyaev & Zeldovich (1972,

¹ <http://wmap.gsfc.nasa.gov/>

² <http://www.rssd.esa.int/Planck>

³ <http://wmap.gsfc.nasa.gov/>

⁴ <http://www.rssd.esa.int/Planck>

1980); Birkinshaw (1999); Rephaeli (1995)) - leaves a characteristic distortion pattern in the CMB spectrum. The fluctuation of this distortion across the sky as probed by CMB observations can provide valuable clues to the fluctuations of the gas density and temperature. The up-scattering in frequency of CMB photons implies an increment in the spectrum at high frequencies with corresponding decrement in the low frequency (Rayleigh-Jeans; RJ) regime, and a null around 217 GHz. This characteristic behaviour is a potential tool for the separation of tSZ from the other temperature anisotropy contributions. Based on the accurate knowledge of tSZ and CMB spectrum foreground removal techniques have been developed to isolate the tSZ signal in the presence of primary anisotropy and instrumental noise. These techniques are extremely effective in subtraction of primary anisotropies due to its well understood (perfect black body) frequency dependence and near Gaussian statistical behaviour (Leach 2008; Bouchet & Gispert 1999; Delabroullie, Cardoso & Patanchon 2003).

The tSZ effect is now routinely imaged in massive galaxy clusters where the temperature of the scattering medium can reach as high as 10KeV. This in effect produces a change in CMB temperature of order 1mK at RJ wavelengths. Individual galaxy cluster tSZ images have a variety of astrophysical and cosmological applications, including direct measurement of the angular diameter distance to the cluster through a combined analysis of X-ray data and measurement of the gas mass which can be useful in estimation of baryon fraction of the Universe. The high frequency instrument of Planck, in particular, has been designed with bands centred at the minimum, the zero, and the maximum of the thermal SZ (tSZ) emission. The extraction of clean CMB and tSZ maps of a catalog of galaxy clusters selected by their tSZ effect are part of scientific programme of Planck. Here we are interested in the general intergalactic medium (IGM) where the gas is expected to be at $\leq 1\text{KeV}$ in the sort of mild overdensities that lead to CMB contributions in the μK range. In this work we primarily focus on the statistical study of wide-field CMB data where tSZ effects lead to anisotropies in the temperature distribution both due to resolved and unresolved galaxy clusters, keeping in mind that the thermal tSZ contribution is the dominant signal beyond the damping tail of the primary anisotropy power spectrum. We primarily focus on analytical modelling of the entire one and the two-point PDF of the tSZ effect.

The tSZ power spectrum is known to be a sensitive probe of the amplitude of density fluctuations. Higher order statistics such as skewness or bispectrum can provide independent estimates on the bias associated with baryonic pressure, as well as providing further consistency checks and cross-validation of lower order estimates. The modelling of lower order statistics of the tSZ effect can be approached in two different ways. The modeling done by various authors (Seljak 2000; Zhang & Pen 2001; Komatsu & Seljak 2001; Zhang & Seth 2007; Cooray 2000, 2001) in the past has followed the halo model (Cooray & Seth 2002). For modeling of the tSZ effect due to photo-ionized gas that traces the dark matter distribution outside collapsed halos we follow Cooray (2001) and use the second order perturbative formalism to model the bispectrum (Goldberg & Spergel 1999a,b). This gas will typically be in a temperature similar to the ionization energy of Hydrogen and Helium. The bias associated with the pressure fluctuations is assumed to be redshift-dependent. For the tSZ effect from collapsed halos the shock heated gas is assumed to be in hydrodynamic equilibrium in virialised halos. The statistical description of halos, including their number count distribution, is assumed to be described by Press-Sechter formalism (Press & Schechter 1974) and their radial profiles to be of NFW form (Navarro, Frenk, White 1996). These ingredients are sufficient for the modelling of the tSZ effect from collapsed halos (Cooray 2000).

In addition to analytical modeling the numerical simulation of tSZ plays an important role in our understanding of the physics involved (Persi et al. 1995; Refregier et al. 2000; Seljak et al. 2000; Springel et al. 2001; White, Hernquist & Springel 2002; Lin et al. 2004; Zhang et al. 2004; Cao, Liu & Fang 2007; Roncarelli et al. 2007; Hallman et al. 2009, 2007; da Silva et al. 1999). Some of these studies incorporate complication from additional radiative and hydrodynamical effects (i.e. ‘‘gastrophysics’’) such as radiative cooling, preheating and SN/AGN feedback to a certain extent. These inputs are otherwise difficult to incorporate in any analytical calculations. On the other hand the simulations too are limited by their dynamic range and can benefit from analytical insights.

In parallel with the development of this PS formalism, analytical modeling based on hierarchical form for the higher order correlation functions has also been studied extensively. In this approach, a specific form of correlation hierarchy is imposed by choosing a generating function that encodes the amplitudes associated with individual vertices. At each order a new hierarchical amplitude appears which can not be expressed in terms of lower order amplitudes. This is a reflection of the fact that gravitational clustering is inherently a non-linear phenomenon. Different hierarchical scenarios differ in the choice of generating functions (Szapudi & Szalay 1993; Szapudi & Colombi 1996; Szapudi & Szalay 1997; Szapudi, Szalay & Boschan 1992). The hierarchical form that is developed in the quasilinear regime and the non-linear regime are different from each other, but reasonably well understood; the intermediate regime remains poorly understood though various fitting functions have been proposed. We employ the particular form proposed by (Balian, Schaeffer 1989) to model the tSZ statistics. This form has been studied extensively in the literature for modeling weak lensing as well for the statistics of collapsed objects and related astrophysical phenomenon. The statistics of collapsed objects and their contribution to the tSZ sky have been studied previously (Valageas & Silk 1999; Valageas, Schaeffer & Silk 2002). These studies also probe X-ray luminosity from the same clusters. In this study we do not probe individual clusters or collapsed objects, but instead directly link the density field with corresponding SZ observables.

For the all-sky experiment Planck (The Planck Collaboration 2006) we consider the range smoothing beams that cover the harmonics (2, 2000). The results are also applicable to the survey Arcminute Cosmology Bolometer Array Receiver (ACBAR; Runyan et al. (2003))⁵ which covers the range (2000, 3000). ACBAR is a multi-frequency millimeter-wave receiver designed for observations of the cosmic microwave back-

⁵ <http://cosmology.berkeley.edu/group/swlh/acbar/>

ground and the Sunyaev-Zel'dovich effect. The ACBAR focal plane consists of a 16 pixel, background-limited, 240 mK bolometer array that can be configured to observe simultaneously at 150, 220, 280, and 350 GHz with 4'-5' FWHM. Together these two experiments will cover the entire range of l values upto 3000.

The paper is organized as follows. In §2 we provide the details of tSZ effect. We link the higher order multispectra of the SZ effect with the underlying mass distribution with the help of various biasing schemes in §3. In §4 we introduce the generic hierarchical *ansatz* and in §5 we introduce the specific formalism based on generating functions in the quasi-linear and highly nonlinear regime. In §6 we show how the PDF and bias of the tSZ sky are related to that of underlying density PDF and bias. Various approximation schemes are discussed that can be used to simplify the PDF and bias. Finally the §7 is dedicated to the discussion of our result and future prospects.

2 FORMALISM

In this section we will provide necessary theoretical background for the computation of lower order moments of tSZ both for the one-point cumulants and the two-point cumulant correlators. These will be later used to construct the entire PDF and the bias of tSZ in the context of hierarchical clustering. We will be using the following form of the Robertson-Walker line element for the background geometry of the universe:

$$d\tau^2 = -c^2 dt^2 + a^2(t)(dr^2 + d_A^2(r)(d\theta^2 + \sin^2\theta d\phi^2)) \quad (1)$$

Where we have denoted angular diameter distance by $d_A(r)$ and scale factor of the universe by $a(t)$. $d_A(r) = K^{-1/2} \sin(K^{-1/2}r)$ for positive curvature, $d_A(r) = (-K)^{-1/2} \sinh((-K)^{-1/2}r)$ for negative curvature and r for the flat universe. For a present value of H_0 and Ω_0 we have $K = (\Omega_0 - 1)H_0^2$. The thermal Sunyaev-Zel'dovich (tSZ) temperature fluctuation $\Delta T(\hat{\Omega}, \nu) = \delta T(\hat{\Omega}, \nu)/T_{\text{CMB}}$ is given by the opacity weighted electron pressure:

$$\Delta T_{\text{SZ}}(\hat{\Omega}, \nu) \equiv g_\nu(x)y(\hat{\Omega}) = \int_0^{r_0} dr \dot{\tau} \pi(\hat{\Omega}, r); \quad \pi(\mathbf{x}) = \delta p_e(\mathbf{x})/\rho_e \quad (2)$$

Here r is the comoving distance, τ is the Thomson optical depth, overdots represent derivatives with respect to r . Here $y(\hat{\Omega})$ is the map of the Compton y -parameter and τ represents the optical depth, which can be expressed in terms the Thomson cross-section σ_T , is the Boltzman constant k_B by the integral $\tau = c \int n_e(z) \sigma_T dt$. The overdot represents the derivative w.r.t. comoving distance r . The free electron number density is represented by $n_e(z)$. The function $g_\nu(x)$ encodes the frequency dependence of the tSZ anisotropies. It relates the temperature fluctuations at a frequency ν with the Compton parameter y . Here the function $g_\nu(x)$ is defined as: $g_\nu(x) = x \coth(x/2) - 4$ with $x = h\nu/(k_B T_{\text{CMB}}) = \nu/(56.84 \text{GHz})$. In the low frequency part of the spectrum $g_\nu(x) = -2$, for $x \ll 1$, here x is the dimensionless frequency as defined above. We will primarily be working in the Fourier domain and will be using the following convention:

$$\pi_e = \frac{\delta p_e}{\rho_e}; \quad \pi_e(\mathbf{k}) = \int d^3\mathbf{x} \pi_e(\mathbf{x}) \exp[-i\mathbf{k} \cdot \mathbf{x}] \quad (3)$$

The projected statistics that we will consider can be related to the 3D statistics which are defined by the following expressions which specify the power spectrum $P_\pi(k)$, the bispectrum $B_\pi(k_1, k_2, k_3)$ and the trispectrum $T_\pi(k_1, k_2, k_3, k_4)$ in terms of the Fourier coefficients.

$$\langle \pi_e(\mathbf{k}_1) \pi_e(\mathbf{k}_2) \rangle_c = (2\pi)^3 P_\pi(k_1) \delta_{\Sigma \mathbf{k}_i=0}; \quad \langle \pi_e(\mathbf{k}_1) \pi_e(\mathbf{k}_2) \pi_e(\mathbf{k}_3) \rangle_c = (2\pi)^3 B_\pi(k_1, k_2, k_3) \delta_{\Sigma \mathbf{k}_i=0}; \quad (4)$$

$$\langle \pi_e(\mathbf{k}_1) \pi_e(\mathbf{k}_2) \pi_e(\mathbf{k}_3) \pi_e(\mathbf{k}_4) \rangle_c = (2\pi)^3 T_\pi(k_1, k_2, k_3, k_4) \delta_{\Sigma \mathbf{k}_i=0} \quad (5)$$

The multispectra of the underlying density field will develop a similar hierarchy. In the linear bias formalism, the multi-spectra of the field π are directly linked to the density contrast $\delta = (\rho - \rho_b)/\rho_b$ with ρ_b being the homogeneous background density of the Universe. Using a bias factor $b_\pi(r)$, which depends on redshift, we can write (Goldberg & Spergel 1999a,b; Cooray 2000, 2001):

$$P_\pi(k_1, r) = b_\pi^2(r) P_\delta(k_1, r); \quad B_\pi(k_1, k_2, k_3; r_i) = b_\pi^3(r) B_\delta(k_1, k_2, k_3; r_i); \quad T_\pi(k_1, k_2, k_3, k_4; r_i) = b_\pi^4(r) T_\delta(k_1, k_2, k_3, k_4; r_i) \quad (6)$$

The time dependence in the bias is typically assumed to be of the following form: $b_\pi(r) = b_\pi(0)/(1+z)$ and $b_\pi(0) = k_B T_e(0) b_\delta / (m_e c^2)$. Various authors have adopted different values for the parameters b_δ and $T_e(0)$. In earlier studies by Seljak et al. (2000) b_δ was found to be in the range 3 to 4 where as (Refregier et al. 2000) found it to be between 8 and 9. The value for $T_e(0)$ in both of these papers are in the range 0.3 – 0.4 KeV. On the other hand Cen & Ostriker (1999) found a higher value $T_e = 1 \text{KeV}$. In (Cooray et al. 2000) this parameter was set to $T_e(0) = 0.5 \text{KeV}$ and $b_\delta = 4$. This leads to $b_\pi = 0.0039$. This is a factor of two smaller compared to the value adopted in (Goldberg & Spergel 1999a). We would like to stress the formalism developed here can take into account any arbitrary functional form for $b_\pi(r)$ and higher order terms that fit the numerical results can also be incorporated; more general functional forms for $b_\pi(r)$ can also be incorporated in our formalism.

The particular cosmology that we will adopt for numerical study are specified by the following parameter values (to be introduced later): $\Omega_\Lambda = 0.741$, $h = 0.72$, $\Omega_b = 0.044$, $\Omega_{\text{CDM}} = 0.215$, $\Omega_M = \Omega_b + \Omega_{\text{CDM}}$, $n_s = 0.964$, $w_0 = -1$, $w_a = 0$, $\sigma_8 = 0.803$, $\Omega_\nu = 0$.

3 LOWER ORDER STATISTICS OF THE THERMAL SZ EFFECT

The statistics of the smoothed tSZ effect $\Theta_{\text{SZ}} = (y_s - \langle y_s \rangle) / \langle y_s \rangle$ reflect those of the projected baryonic pressure fluctuations along the line of sight. In our analysis we will consider a small patch of the sky where we can use the plane parallel approximation or small angle approximation to replace spherical harmonics by Fourier modes. The three-dimensional pressure fluctuations π along the line of sight when projected onto the sky with the weight function $\omega_{\text{SZ}}(r)$ gives the SZ effect in a direction $\hat{\Omega}$ which we denote by $\Theta_{\text{SZ}}(\hat{\Omega})$:

$$\Theta_{\text{SZ}}(\hat{\Omega}) = \int_0^{r_s} dr \omega_{\text{SZ}}(r) \pi(r, \hat{\Omega}); \quad \omega_{\text{SZ}}(r) = -2\dot{\tau}(r) \quad (7)$$

here $d_A(r)$ is the angular diameter distance at a comoving distance r . Using the Fourier transform of π , $\Theta_{\text{SZ}}(\hat{\Omega})$ can be expressed as:

$$\Theta_{\text{SZ}}(\hat{\Omega}) = \int_0^{r_s} dr \omega_{\text{SZ}}(r) \int \frac{d^3\mathbf{k}}{(2\pi)^3} \exp(irk_{\parallel} + id_A(r)\theta_{12} \cdot \mathbf{k}_{\perp}) \pi(\mathbf{k}, r), \quad (8)$$

where θ_{12} denotes the angle between the line of sight direction $\hat{\Omega}$ and should be treated as a vector on the surface of the sky and the wave vector \mathbf{k} , k_{\parallel} and \mathbf{k}_{\perp} denote the components of \mathbf{k} , parallel and perpendicular to the line of sight direction. In the small angle approximation one assumes that $|\mathbf{k}_{\perp}| \gg k_{\parallel}$. Using these definitions we can compute the projected two-point correlation function in terms of the dark matter power spectrum $P_{\delta}(k, r)$ (Peebles 1980; Kaiser 1992; Kaiser 1998):

$$\langle \Theta_{\text{SZ}}(\hat{\Omega}_1) \Theta_{\text{SZ}}(\hat{\Omega}_2) \rangle_c = \int_0^{r_s} dr \frac{\omega_{\text{SZ}}^2(r)}{d_A^2(r)} \int \frac{d^2\mathbf{l}}{(2\pi)^2} \exp(\theta_{12} \cdot \mathbf{l}) P_{\pi} \left[\frac{l}{d_A(r)}, r \right]. \quad (9)$$

Here θ_{12} is the angular separation projected onto the surface of the sky and we have also introduced $\mathbf{l} = d_A(r)\mathbf{k}_{\perp}$ to denote the scaled projected wave vector. Using Limber's approximation, the variance of Θ_{SZ} smoothed using a Gaussian beam $b_l(\theta_b)$ with FWHM = θ_b can be written as:

$$\langle \Theta_{\text{SZ}}^2(\theta_b) \rangle = \int_0^{r_s} dr \frac{\omega_{\text{SZ}}^2(r)}{d_A^2(r)} \int \frac{d^2\mathbf{l}}{(2\pi)^2} P_{\pi} \left(\frac{l}{d_A(r)}, r \right) b_l^2(\theta_b) \quad (10)$$

Similarly the higher order moments of the smoothed temperature field relate $\langle \Theta_{\text{SZ}}^p(\theta_b) \rangle$ to the three-dimensional multi-spectra of the underlying dark matter distribution B_p (Hui 1999; Munshi & Coles 1999a):

$$\langle \Theta_{\text{SZ}}^3(\theta_b) \rangle_c = \int_0^{r_s} dr \frac{\omega_{\text{SZ}}^3(r)}{d_A^3(r)} \int \frac{d^2\mathbf{l}_1}{(2\pi)^3} b_{l_1}(\theta_b) \int \frac{d^2\mathbf{l}_2}{(2\pi)^2} b_{l_2}(\theta_b) \int \frac{d^2\mathbf{l}_3}{(2\pi)^3} b_{l_3}(\theta_b) B_{\pi} \left(\frac{l_i}{d_A(r)} \right) \quad (11)$$

$$\langle \Theta_{\text{SZ}}^4(\theta_b) \rangle_c = \int_0^{r_s} dr \frac{\omega_{\text{SZ}}^4(r)}{d_A^4(r)} \int \frac{d^2\mathbf{l}_1}{(2\pi)^3} b_{l_1}(\theta_b) \cdots \int \frac{d^2\mathbf{l}_4}{2\pi^2} b_{l_4}(\theta_b) T_{\pi} \left(\frac{l_i}{d_A(r)} \right) \quad (12)$$

We will use these results to show that it is possible to compute the complete probability distribution function of Θ_{SZ} from the underlying dark matter probability distribution function. Details of the analytical results presented here can be found in Munshi & Coles (1999b). Similar analysis for the higher order cumulant correlators (Szapudi & Szalay 1997; Munshi & Coles 1999) of the smoothed SZ field relating $\langle \Theta_{\text{SZ}}^p(\hat{\Omega}_1) \Theta_{\text{SZ}}^q(\hat{\Omega}_2) \rangle_c$ with multi-spectra of underlying dark matter distribution B_{p+q} can be expressed as (Munshi & Coles 1999a):

$$\langle \Theta_{\text{SZ}}^2(\hat{\Omega}_1) \Theta_{\text{SZ}}(\hat{\Omega}_2) \rangle_c = \int_0^{r_s} \frac{\omega_{\text{SZ}}^3(r)}{d_A^4(r)} dr \int \frac{d^2\mathbf{l}_1}{(2\pi)^2} \int \frac{d^2\mathbf{l}_2}{(2\pi)^2} b_{l_1}(\theta_b) b_{l_2}(\theta_b) b_{l_3}(\theta_b) \exp(il_2 \cdot \theta_{12}) B_{\pi} \left(\frac{\mathbf{l}_i}{d_A(r)} \right)_{\Sigma \mathbf{l}_i=0}; \quad (13)$$

$$\langle \Theta_{\text{SZ}}^3(\hat{\Omega}_1) \Theta_{\text{SZ}}(\hat{\Omega}_2) \rangle_c = \int_0^{r_s} \frac{\omega_{\text{SZ}}^4(r)}{d_A^6(r)} dr \int \frac{d^2\mathbf{l}_1}{(2\pi)^2} \int \frac{d^2\mathbf{l}_2}{(2\pi)^2} \int \frac{d^2\mathbf{l}_3}{(2\pi)^2} b_{l_1}(\theta_b) \cdots b_{l_4}(\theta_b) \exp(il_3 \cdot \theta_{12}) T_{\pi} \left(\frac{\mathbf{l}_i}{d_A(r)} \right)_{\Sigma \mathbf{l}_i=0}$$

$$\langle \Theta_{\text{SZ}}^2(\hat{\Omega}_1) \Theta_{\text{SZ}}^2(\hat{\Omega}_2) \rangle_c = \int_0^{r_s} \frac{\omega_{\text{SZ}}^3(r)}{d_A^6(r)} dr \int \frac{d^2\mathbf{l}_1}{(2\pi)^2} \cdots \int \frac{d^2\mathbf{l}_4}{(2\pi)^2} b_{l_1}(\theta_b) \cdots b_{l_4}(\theta_b) \exp(i(l_1 + l_2) \cdot \theta_{12}) T_{\pi} \left(\frac{\mathbf{l}_i}{d_A(r)} \right)_{\Sigma \mathbf{l}_i=0}. \quad (14)$$

We will use and extend these results in this paper to show that it is possible to compute the entire bias function $b(> \Theta_{\text{SZ}})$, i.e. the bias associated with those spots in the tSZ map which Θ_{SZ} is above certain threshold from the statistics of underlying over-dense dark objects; this then acts as a generating function for the cumulant correlators. Details of analytical results presented here can be found in Munshi & Coles (1999b).⁶

⁶ <http://mwhite.berkeley.edu/tSZ/>

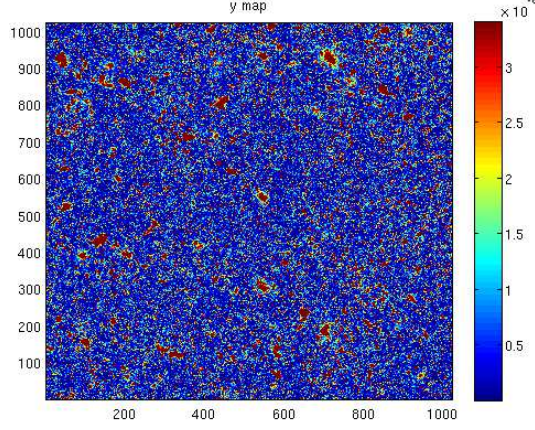


Figure 1. A simulated map of y-sky used in our study. These simulations were generated for Planck related studies. The maps are 10 degree on a side and were generated on a 1024×1024 grid. More details about the simulations can be found in (White 2003).

4 HIERARCHICAL ANSATZE

The spatial length scales corresponding to the small angular scales of relevance here are in the highly non-linear regime. Assuming a *tree model* for the matter correlation hierarchy in the highly non-linear regime, one can write the general form of the N th order correlation function $\xi_\delta^{(N)}$ as (Groth & Peebles 1977, Fry & Peebles 1978, Davis & Peebles 1983, Bernardeau & Schaeffer 1992, Szapudi & Szalay 1993):

$$\xi_\delta^{(N)}(\mathbf{r}_1, \dots, \mathbf{r}_N) = \sum_{\alpha, N\text{-trees}} Q_{N,\alpha} \sum_{\text{labellings}} \prod_{\text{edges}} \xi_\delta^{(2)}(\mathbf{r}_i, \mathbf{r}_j). \quad (15)$$

It is interesting to note that a similar hierarchy develops in the quasi-linear regime in the limit of vanishing variance (Bernardeau 1992). However the hierarchical amplitudes $Q_{N,\alpha}$ become shape-dependent functions in the quasi-linear regime. In the highly nonlinear regime there are some indications that these functions become independent of shape, as suggested by studies of the lowest order parameter $Q_3 = Q$ using high resolution numerical simulations (Scoccimarro et al. 1998). In Fourier space such an *ansatz* means that the hierarchy of multi-spectra can be written as sums of products of the matter power-spectrum:

$$\begin{aligned} B_\delta(\mathbf{k}_1, \mathbf{k}_2, \mathbf{k}_3)_{\sum k_i=0} &= Q(P_\delta(k_1)P_\delta(k_2) + P_\delta(k_2)P_\delta(k_3) + P_\delta(k_3)P_\delta(k_1)) \\ T_\delta(\mathbf{k}_1, \mathbf{k}_2, \mathbf{k}_3, \mathbf{k}_4)_{\sum k_i=0} &= R_a P_\delta(k_1)P_\delta(|\mathbf{k}_1 + \mathbf{k}_2|)P_\delta(|\mathbf{k}_1 + \mathbf{k}_2 + \mathbf{k}_3|) + \text{cyc.perm.} + R_b P_\delta(k_1)P_\delta(k_2)P_\delta(k_3) + \text{cyc.perm.} \end{aligned} \quad (16)$$

Different hierarchical models differ in the way they predict the amplitudes of different tree topologies. Bernardeau & Schaeffer (1992) considered the case where amplitudes in general are factorizable, at each order one has a new “star” amplitude and higher order “snake” and “hybrid” amplitudes can be constructed from lower order “star” amplitudes; see Munshi, Melott & Coles (1999a,b,c) for a detailed description. In the models proposed by Szapudi & Szalay (1993) it was assumed that all hierarchical amplitudes of any given order are degenerate. Galaxy surveys have been used to study these *ansatze*. Our goal here is to show that tSZ surveys can also provide valuable information in this direction, in addition to constraining the matter power-spectra and background geometry of the universe. We will use the model proposed by Bernardeau & Schaeffer (1992) and its generalization to the quasi-linear regime by Bernardeau (1992, 1994) to construct the PDF of the tSZ field $\Theta(\theta_0)$. We express the one-point cumulants as:

$$\langle \Theta_{\text{SZ}}^3(\theta_b) \rangle = (3Q_3)C_3[\Theta_{\theta_b}^2] = S_3^{\text{SZ}} \langle \Theta_{\text{SZ}}^2(\theta_b) \rangle^2 \quad \langle \Theta_{\text{SZ}}^4(\theta_b) \rangle = (12R_a + 4R_b)C_4[\Theta_{\theta_b}^3] = S_4^{\text{SZ}} \langle \Theta_{\text{SZ}}^2(\theta_b) \rangle^3, \quad (17)$$

where we have introduced the following equation:

$$C_p [[\Theta_{\theta_b}]^{p-1}] = \int_0^{r_s} \frac{\omega^p(r) b_\pi^p(r)}{d_A^{2(p-1)}(r)} [\Theta_{\theta_b}]^{(p-1)} dr; \quad [\Theta_{\theta_b}] = \int \frac{d^2\mathbf{l}}{(2\pi)^2} P_\delta \left(\frac{l}{d_A(r)} \right) b_l^2(\theta_b). \quad (18)$$

Equation (17) was derived by Hui (1998) in the context of weak lensing surveys. He showed that his result agrees well with the ray tracing simulations of Jain, Seljak and White (1998). Later studies extended this result to the entire family of two-point statistics such as cumulant correlators (Munshi & Coles 1999, Munshi & Jain 1999).

$$\langle \Theta_{SZ}^2(\hat{\Omega}_1) \Theta_{SZ}(\hat{\Omega}_2) \rangle_c = 2Q_3 C_3[\Theta_{\theta_b} \Theta_{\theta_{12}}] = C_{21}^\eta C_3[\Theta_{\theta_b} \Theta_{\theta_{12}}] \equiv C_{21}^{SZ} \langle \Theta_{SZ}^2 \rangle_c \langle \Theta_{SZ}(\hat{\Omega}_1) \Theta_{SZ}(\hat{\Omega}_2) \rangle_c, \quad (19)$$

$$\langle \Theta_{SZ}^3(\hat{\Omega}_1) \Theta_{SZ}(\hat{\Omega}_2) \rangle_c = (3R_a + 6R_b) C_4[\Theta_{\theta_b}^2 \Theta_{\theta_{12}}] = C_{31}^\eta C_4[\Theta_{\theta_b}^2 \Theta_{\theta_{12}}] \equiv C_{31}^{SZ} \langle \Theta_{SZ}^2 \rangle_c^2 \langle \Theta_{SZ}(\hat{\Omega}_1) \Theta_{SZ}(\hat{\Omega}_2) \rangle_c, \quad (20)$$

$$\langle \Theta_{SZ}^2(\hat{\Omega}_1) \Theta_{SZ}^2(\hat{\Omega}_2) \rangle_c = 4R_b C_4[\Theta_{\theta_b}^2 \Theta_{\theta_{12}}] = C_{22}^\eta C_4[\Theta_{\theta_b} \Theta_{\theta_{12}}] \equiv C_{22}^{SZ} \langle \Theta_{SZ}^2 \rangle_c^2 \langle \Theta_{SZ}(\hat{\Omega}_1) \Theta_{SZ}(\hat{\Omega}_2) \rangle_c, \quad (21)$$

$$\langle \Theta_{SZ}^4(\hat{\Omega}_1) \Theta_{SZ}(\hat{\Omega}_2) \rangle_c = (24S_a + 36S_b + 4S_c) C_5[\Theta_{\theta_b}^3 \Theta_{\theta_{12}}] = C_{41}^\eta C_5[\Theta_{\theta_b}^3 \Theta_{\theta_{12}}] \equiv C_{41}^{SZ} \langle \Theta_{SZ}^2 \rangle_c^3 \langle \Theta_{SZ}(\hat{\Omega}_1) \Theta_{SZ}(\hat{\Omega}_2) \rangle_c, \quad (22)$$

$$\langle \Theta_{SZ}^3(\hat{\Omega}_1) \Theta_{SZ}^2(\hat{\Omega}_2) \rangle_c = (12S_a + 6S_b) C_5[\Theta_{\theta_b}^3 \Theta_{\theta_{12}}] = C_{32}^\eta C_5[\Theta_{\theta_b}^3 \Theta_{\theta_{12}}] \equiv C_{32}^{SZ} \langle \Theta_{SZ}^2 \rangle_c^3 \langle \Theta_{SZ}(\hat{\Omega}_1) \Theta_{SZ}(\hat{\Omega}_2) \rangle_c. \quad (23)$$

where C_{pq}^η denotes the cumulant correlators for the underlying mass distribution,

$$C_p[[\Theta_{\theta_0}]^p \Theta_{\theta_{12}}] = \int_0^{r_s} \frac{\omega_{SZ}^p(r) b^p(r)}{d_A^{2(p-1)}(r)} [\Theta_{\theta_0}^{SZ}]^p [\Theta_{\theta_{12}}] dr; \quad \Theta_{\theta_{12}} \equiv \int \frac{d^2\mathbf{l}}{(2\pi)^2} P_\delta \left(\frac{l}{d_A(r)} \right) b_l^2(\theta_0) \exp(\mathbf{l} \cdot \theta_{12}). \quad (24)$$

These lowest order statistics can be helpful in probing the pressure bias as a function of scale. It is however expected that the signal to noise will decrease with increasing order. We will use these results to construct the entire PDF and the bias associated with the tSZ maps. This will be achieved using a generating function approach.

5 THE GENERATING FUNCTION

In scaling analysis of the probability distribution function (PDF) the void probability distribution function (VPF) plays a most fundamental role, because it can be related to the generating function $\phi(y)$ of the cumulants or, if preferred, the S_N parameters (White 1979; Balian & Schaeffer 1989):

$$P_v(0) = \exp(-\bar{N}\sigma(N_c)) = \exp\left(-\frac{\phi(N_c)}{\xi_2}\right), \quad (25)$$

where $P_v(0)$ is the probability of having no ‘‘particles’’ in a cell of volume v , \bar{N} is the average occupancy of these ‘‘particles’’ and $N_c = \bar{N}\xi_2$. The VPF is meaningful only for discrete distribution of particles and can not be defined for smooth density fields such as δ or $\kappa(\theta_0)$. However the scaling functions defined above $\sigma(y) = -\phi(y)/y$ are very much useful even for continuous distributions where they can be used as a generating function of one-point cumulants or S_p parameters: $\phi(y) = \sum_{p=1}^{\infty} S_p/p!y^p$. The function $\phi(y)$ satisfies the constraint $S_1 = S_2 = 1$ necessary for proper normalization of the PDF. The other generating function which plays a very important role in such analysis is the generating function for vertex amplitudes ν_n , associated with nodes appearing in tree representation of higher order correlation hierarchy ($Q_3 = \nu_2$, $R_a = \nu_2^2$ and $R_b = \nu_3$). In practice it is possible to work with a perturbative expansion of the vertex generating function $\mathcal{G}(\tau)$. In terms of the vertices it is defined as: $\mathcal{G}(\tau) = \sum_{n=0}^{\infty} (-1)^n \nu_n/n!$. However in the highly nonlinear regime a closed form is used. A more specific model for $\mathcal{G}(\tau)$, which is useful to make more specific predictions (Bernardeau & Schaeffer 1979) is given by $\mathcal{G}(\tau) = \left(1 + \tau/\kappa_a\right)^{-\kappa_a}$. We will relate κ_a with other parameters of scaling models. While the definition of VPF do not use any specific form of hierarchical *ansatz* it is to realize that writing the tree amplitudes in terms of the weights associated with nodes is only possible when one assumes a factorizable model for tree hierarchy (Bernardeau & Schaeffer 1992) and other possibilities which do not violate the assumption of a tree model are also possible (Bernardeau & Schaeffer 1999). The generating functions for tree nodes can be related to the VPF by solving a pair of implicit equations (Balian & Schaeffer 1989),

$$\phi(y) = y\mathcal{G}(\tau) - \frac{1}{2}y\tau \frac{d}{d\tau} \mathcal{G}(\tau); \quad \tau = -y \frac{d}{d\tau} \mathcal{G}(\tau). \quad (26)$$

However a more detailed analysis is needed to include the effect of correlation between two or more correlated volume elements which will provide information about bias, cumulants and cumulant correlators of these collapsed object (as opposed to the cumulants and cumulant correlators of the whole map, e.g. Munshi & Jain (1999a)). We will only quote results useful for measurement of bias; detailed derivations of related results including related error analysis can be found elsewhere (Bernardeau & Schaeffer 1992, 1999; Munshi et al. 1999a,b,c; Coles et al. 1999). Notice that $\tau(y)$ (also denoted by $\beta(y)$ in the literature) plays the role of a generating function for factorized cumulant correlators C_{p1} ($C_{pq} = C_{p1}C_{q1}$): $\tau(y) = \sum_{p=1}^{\infty} C_{p1}/p!y^p$. We will next consider two different regimes. The quasi-linear regime valid at large angular scales and the highly nonlinear regime valid at smaller angular scales.

5.1 The Highly Non-linear Regime

The PDF $p(\delta)$ and bias $b(\delta)$ can be related to their generating functions VPF $\phi(y)$ and $\tau(y)$ respectively by following equations (Balian & Schaeffer 1989, Bernardeau & Schaeffer 1992, Bernardeau & Schaeffer 1999) ⁷,

$$p(\delta) = \int_{-i\infty}^{i\infty} \frac{dy}{2\pi i} \exp \left[\frac{(1+\delta)y - \phi(y)}{\xi_2} \right]; \quad b(\delta)p(\delta) = \int_{-i\infty}^{i\infty} \frac{dy}{2\pi i} \tau(y) \exp \left[\frac{(1+\delta)y - \phi(y)}{\xi_2} \right]. \quad (27)$$

It is clear that the function $\phi(y)$ completely determines the behavior of the PDF $p(\delta)$ for all values of δ . However different asymptotic expressions of $\phi(y)$ govern the behavior of $p(\delta)$ for different intervals of δ . For large y we can express $\phi(y)$ as: $\phi(y) = ay^{1-\omega}$. Where we have introduced a new parameter ω for the description of VPF. This parameter plays a very important role in scaling analysis. No theoretical analysis has been done so far to link ω with initial power spectral index n . Numerical simulations are generally used to fix ω for a specific initial condition. Such studies have confirmed that the increase in power on smaller scales increases the value of ω . Typically initial power spectrum with spectral index $n = -2$ (which should model CDM like spectra we considered in our simulations at small length scales) produces a value of .3 which we will be using in our analysis of PDF (Colombi et. al. (1992, 1994, 1995). The VPF $\phi(y)$ and its two-point analog $\tau(y)$ both exhibit singularity for small but negative value of y_s ,

$$\phi(y) = \phi_s - a_s \Gamma(\omega_s)(y - y_s)^{-\omega_s}; \quad \tau(y) = \tau_s - b_s(y - y_s)^{-\omega_s-1}. \quad (28)$$

For the factorizable model of the hierarchical clustering the parameter ω_s takes the value $-3/2$ and a_s and b_s can be expressed in terms of the nature of the generating function $\mathcal{G}(\tau)$ and its derivatives near the singularity τ_s (Bernardeau & Schaeffer 1992):

$$a_s = \frac{1}{\Gamma(-1/2)} \mathcal{G}'(\tau_s) \mathcal{G}''(\tau_s) \left[\frac{2\mathcal{G}'(\tau_s)\mathcal{G}''(\tau_s)}{\mathcal{G}'''(\tau_s)} \right]^{3/2}; \quad b_s = \left[\frac{2\mathcal{G}'(\tau_s)\mathcal{G}''(\tau_s)}{\mathcal{G}'''(\tau_s)} \right]^{1/2}. \quad (29)$$

As mentioned before the parameter k_a which we have introduced in the definition of $\mathcal{G}(\tau)$ can be related to the parameters a and ω appearing in the asymptotic expressions of $\phi(y)$ (Balian & Schaeffer 1989, Bernardeau & Schaeffer 1992),

$$\omega = k_a/(k_a + 2); \quad a = \frac{k_a + 2}{2} k_a^{k_a/(k_a+2)}. \quad (30)$$

Similarly the parameter y_s which describe the behavior of the function $\phi(y)$ near its singularity can be related to the behavior of $\mathcal{G}(\tau)$ near τ_s which is the solution of the equation (Balian & Schaeffer 1989, Bernardeau & Schaeffer 1992), $\tau_s = \mathcal{G}'(\tau_s)/\mathcal{G}''(\tau_s)$, finally we can relate k_a to y_s by following expression (see eq. (30)): $y_s = -\tau_s/\mathcal{G}'(\tau_s)$, or we can write:

$$-\frac{1}{y_s} = x_* = \frac{1}{k_a} \frac{(k_a + 2)^{k_a+2}}{(k_a + 1)^{k_a+1}}. \quad (31)$$

The newly introduced variable x_* will be useful to define large δ tail of the PDF $p(\delta)$ and the bias $b(\delta)$. Different asymptotes in $\phi(y)$ are linked with behavior of $p(\delta)$ for various regimes of δ . For very large values of variance i.e. ξ_2 it is possible to define a scaling function $p(\delta) = \frac{1}{\xi_2} h(x)$ which will encode the scaling behavior of PDF, where plays the role of the scaling variable and is defined as $\frac{1+\delta}{\xi_2}$. We list different ranges of δ and specify the behavior of $p(\delta)$ and $b(\delta)$ in these regimes (Balian & Schaeffer 1989).

$$\bar{\xi}^{-\frac{\omega}{1-\omega}} \ll 1 + \delta \ll \bar{\xi}; \quad p(\delta) = \frac{a}{\xi_2^2} \frac{1-\omega}{\Gamma(\omega)} \left(\frac{1+\delta}{\xi_2} \right)^{\omega-2}; \quad b(\delta) = \left(\frac{\omega}{2a} \right)^{1/2} \frac{\Gamma(\omega)}{\Gamma[\frac{1}{2}(1+\omega)]} \left(\frac{1+\delta}{\bar{\xi}} \right)^{(1-\omega)/2} \quad (32)$$

$$1 + \delta \gg \bar{\xi}_2; \quad p(\delta) = \frac{a_s}{\bar{\xi}_2^2} \left(\frac{1+\delta}{\bar{\xi}_2} \right) \exp \left(-\frac{1+\delta}{x_* \bar{\xi}_2} \right); \quad b(\delta) = -\frac{1}{\mathcal{G}'(\tau_s)} \frac{(1+\delta)}{\bar{\xi}_2} \quad (33)$$

The integral constraints satisfied by these scaling functions are $S_1 = \int_0^\infty xh(x)dx = 1$ and $S_2 = \int_0^\infty x^2h(x)dx = 1$. These take care of normalization of the function $p(\delta)$. Similarly the normalization constraint over $b(\delta)$ can be expressed as $C_{11} = \int_0^\infty xb(x)h(x)dx = 1$, which translates into $\int_{-1}^\infty d\delta b(\delta)p(\delta) = 0$ and $\int_{-1}^\infty d\delta b(\delta)p(\delta) = 1$. Several numerical studies have been conducted to study the behavior of $h(x)$ and $b(x)$ for different initial conditions (e.g. Colombi et al. 1992,1994,1995; Munshi et al. 1999; Valageas et al. 1999). For very small values of δ the behavior of $p(\delta)$ is determined by the asymptotic behavior of $\phi(y)$ for large values of y , and it is possible to define another scaling function $g(z)$

⁷ We will use the symbol y to denote the dummy variable below. However this is not related to the y parameter defined before to describe the tSZ effect. The y_s defined here is the singular value of the dummy variable y in the complex plane.

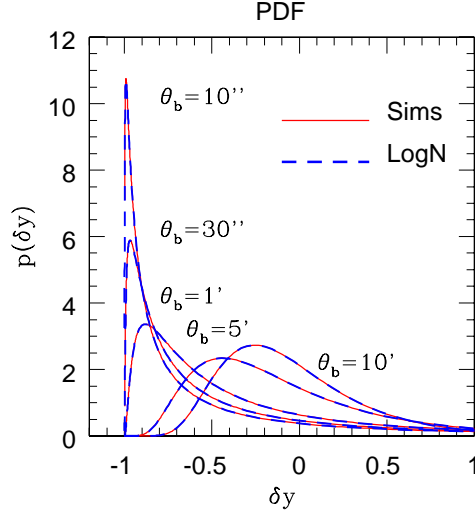


Figure 2. The pdf $p(\delta y)$ as recovered from simulations is plotted as a function of $\delta y = y/\langle y \rangle - 1$. The beams we have considered correspond to FWHM $\theta_b = 10'', 30'', 1', 5', 10'$ as indicated. Various curves correspond to results from simulations (solid), log-normal distribution (short-dashed).

which is completely determined by ω , the scaling parameter can be expressed as $z = (1 + \delta)a^{-1/(1-\omega)}\bar{\xi}_2^{\omega/(1-\omega)}$. However numerically it is much easier to determine ω from the study of $\sigma(y)$ compared to the study of $g(z)$ (e.g. Bouchet & Hernquist 1992).

$$1 + \delta \ll \bar{\xi}_2; \quad p(\delta) = a^{-1/(1-\omega)}\bar{\xi}_2^{\omega/(1-\omega)}\sqrt{\frac{(1-\omega)^{1/\omega}}{2\pi\omega z^{(1+\omega)/\omega}}}\exp\left[-\omega\left(\frac{z}{1-\omega}\right)^{-(1-\omega)/\omega}\right]; \quad b(\delta) = -\left(\frac{2\omega}{\bar{\xi}_2}\right)^{1/2}\left(\frac{1-\omega}{z}\right)^{(1-\omega)/2\omega} \quad (34)$$

To summarize, we can say that the entire behavior of the PDF $P(\delta)$ is encoded in two different scaling functions, $h(x)$ and $g(z)$ and one can also study the scaling properties of $b(\delta)$ in terms of the scaling variables x and z in a very similar way. These scaling functions are relevant for small and large δ behavior of the function $p(\delta)$ and $b(\delta)$. Typically the PDF $p(\delta)$ shows a cutoff at both large and small values of δ and it exhibits a power-law in the middle. The power law behavior is observed when both $g(z)$ and $h(x)$ overlap and is typical of highly non-linear regime. With the decrease in $\bar{\xi}_2$ the range of δ for which $p(\delta)$ shows such a power law behavior decreases finally to vanish for the case of very small variance i.e. in the quasi-linear regime. Similarly the bias is very small and a slowly varying function for moderately over dense objects but increases rapidly for over dense objects which are in qualitative agreement with PS formalism.

5.2 The Quasi-linear Regime

In the quasi-linear regime, a similar formalism can be used to study the PDF. However the generating function can now be explicitly evaluated using tree-level perturbative dynamics (Bernardeau 1992; Munshi, Sahni, Starobinsky 1994; Bernardeau 1994). It is also possible to take smoothing corrections into account in which case one can have explicit expression of ω in terms of the initial power spectral index n . In general the parameters k_a or ω characterising VPF or CPDF are different from their highly non-linear values.

For the purpose of our calculations it is important to notice that although the generating function for the matter correlation hierarchy for very small angular smoothing is the same as the highly non-linear regime, the analytical results that are useful are those from the quasi-linear regime as the variance of projected density field remains very small even for small smoothing scales. The PDF and bias now can be expressed in terms of $G_\delta(\tau)$ (Bernardeau 1992; Munshi, Sahni, Starobinsky 1994; Bernardeau 1994):

$$p(\delta)d\delta = \frac{1}{-G'_\delta(\tau)}\left[\frac{1 - \tau G''_\delta(\tau)/G'_\delta(\tau)}{2\pi\bar{\xi}_2}\right]^{1/2}\exp\left(-\frac{\tau^2}{2\bar{\xi}_2}\right)d\tau; \quad b(\delta) = -\left(\frac{k_a}{\bar{\xi}_2}\right)\left[(1 + G_\delta(\tau))^{1/k_a} - 1\right], \quad (35)$$

$$G_\delta(\tau) = \mathcal{G}(\tau) - 1 = \delta. \quad (36)$$

The above expression is valid for $\delta < \delta_c$ where the δ_c is the value of δ which cancels the numerator of the pre-factor of the exponential function appearing in the above expression. For $\delta > \delta_c$ the PDF develops an exponential tail which is related to the presence of singularity in $\phi(y)$ in a

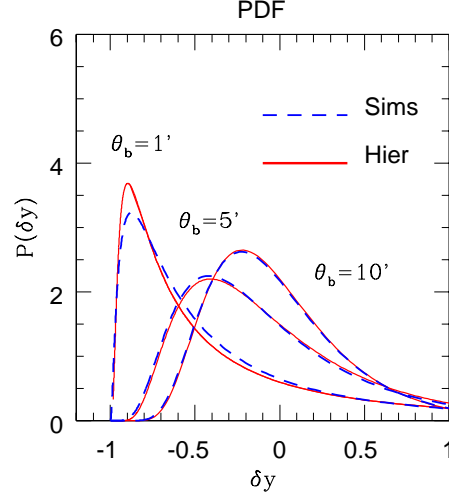


Figure 3. The predictions from hierarchical ansatz are displayed against results from numerical simulations. Three different beams are displayed with $\theta_b = 1', 5', 10'$ respectively. The perturbative calculation breaks down for smaller beam size as the variance is higher than unity.

very similar way as in the case of its highly non-linear counterpart (Bernardeau 1992, Bernardeau 1994):

$$p(\delta)d\delta = \frac{3a_s\sqrt{\xi_2}}{4\sqrt{\pi}}\delta^{-5/2}\exp\left[-|y_s|\frac{\delta}{\xi_2} + \frac{|\phi_s|}{\xi_2}\right]d\delta; \quad b(\delta) = -\frac{1}{\mathcal{G}'(\tau_s)}\frac{(1+\delta)}{\xi_2}. \quad (37)$$

It may be noted that similar analytical expressions for the PDF and bias can also be derived for the case of approximate dynamics sometime used to simulate gravitational clustering in the weakly non-linear regime or to reconstruct the projected density maps from convergence maps in the context of weak lensing surveys with large smoothing angles (e.g. Lagrangian perturbation theory which is an extension of Zeldovich approximation (Munshi, Sahni, Starobinsky 1994)).

6 THE PDF AND THE BIAS OF BEAM SMOOTHED SZ EFFECT

For computing the probability distribution function of the smoothed scaled tSZ field $\tilde{\Theta}_{\text{SZ}}(\theta_b) = \Theta_{\text{SZ}}(\theta_b)/\bar{\Theta}_{\text{SZ}}(\theta_b)$, we will begin by constructing its associated cumulant generating function $\Phi_{\tilde{\Theta}}(y)$:

$$\Phi_{\tilde{\Theta}(\theta_b)}(y) = \sum_{p=1}^{\infty} \frac{\langle \tilde{\Theta}_{\text{SZ}}^p(\theta_b) \rangle}{\langle \tilde{\Theta}_{\text{SZ}}^2(\theta_b) \rangle^{p-1}} y^p \quad (38)$$

Notice that the construction already satisfies the constraint equation $S_1 = S_2 = 1$. Now using the expressions for the higher moments of the SZ in terms of the matter power spectrum (Eq.(10) and Eq.(18)) gives:

$$\Phi_{\tilde{\Theta}(\theta_b)}(y) \equiv \sum_{p=1}^{\infty} \frac{S_p^{\tilde{\Theta}}}{p!} y^p = \int_0^{r_s} \sum_{p=1}^{\infty} \frac{1}{p!} S_p^{\text{SZ}} \frac{b_{\pi}^p(r)\omega_{\text{SZ}}^p(r)}{d_A(r)^{2(p-1)}(r)} \mathcal{I}_{\theta_b}^{(p-1)} \frac{y^p}{\langle \Theta_{\text{SZ}}^2(\theta_b) \rangle^{(p-1)}}. \quad (39)$$

We can now use the definition of $\phi(y)$ for the matter cumulants to express $\Phi_{\tilde{\Theta}(\theta_b)}(y)$, in terms of $\phi(y)$:

$$\Phi_{\tilde{\Theta}(\theta_b)}(y) = \int_0^{r_s} dr \left[\frac{d_A^2(r)\langle \Theta_{\text{SZ}}^2(\theta_b) \rangle}{\Theta_{\text{SZ}}(\theta_b)\mathcal{I}_{\theta_b}} \right] \phi \left[\bar{\Theta}_{\text{SZ}}(\theta_b) b_{\pi}(r) \frac{\omega_{\text{SZ}}(r)}{d_A^2(r)} \frac{\mathcal{I}_{\theta_b}}{\langle \Theta_{\text{SZ}}^2(\theta_b) \rangle} y \right] \quad (40)$$

Note that we have used the fully non-linear generating function ϕ for the cumulants, though we will use it to construct a generating function in the quasi-linear regime. The analysis becomes much easier if we define a new scaled tSZ field $\eta(\theta_b) = 1 + \delta\Theta_{\text{SZ}}$:

$$\eta_{\text{SZ}}(\theta_b) = \Theta_{\text{SZ}}(\theta_b)/\bar{\Theta}_{\text{SZ}}(\theta_b) \quad (41)$$

With the reduced SZ field η , the cumulant generating function is given by,

$$\Phi_{\tilde{\Theta}}(y) = \frac{1}{\tilde{\Theta}_{\text{SZ}}} \int_0^{r_s} dr \left[\frac{d_A^2(r)}{\tilde{\Theta}_{\text{SZ}}(\theta_b)} \frac{\langle \Theta_{\text{SZ}}^2(\theta_b) \rangle}{\mathcal{I}_{\theta_b}} \right] \phi \left[b_\pi(r) \tilde{\Theta}_{\text{SZ}} \frac{y}{\langle \Theta_{\text{SZ}}^2 \rangle} \frac{w_{\text{SZ}}(r)}{d_A^2(r)} \mathcal{I}_{\theta_b} \right] \quad (42)$$

The scaling function $h(x)$ for η associated with the PDF $P(\eta)$ can now be easily related with the matter scaling function $h(x)$ introduced earlier:

$$h_{\tilde{\Theta}}(x) = - \int_{-\infty}^{\infty} \frac{dy}{2\pi i} \exp(xy) \Phi_{\tilde{\Theta}}(y). \quad (43)$$

Using this definition we can write:

$$h_{\tilde{\Theta}}(x) = \int_0^{r_s} dr \frac{w_{\text{SZ}}(r)}{\tilde{\Theta}_{\text{SZ}}(\theta_b)} \left[\frac{d_A^2(r)}{\tilde{\Theta}_{\text{SZ}}} \frac{\langle \Theta^2(\theta_b) \rangle}{\mathcal{I}_{\theta_b}} \right]^2 h \left[\tilde{\Theta}_{\text{SZ}} \frac{x}{\langle \Theta^2 \rangle} \frac{w_{\text{SZ}}}{d_A^2(r)} \mathcal{I}_{\theta_b} \right]. \quad (44)$$

While the expressions derived above are exact and are derived for the most general case using only the small angle approximation, they can be simplified considerably using further approximations. In the following we will assume that the contribution to the r integrals can be replaced by an average value coming from the maximum of $\omega_{\text{SZ}}(r)$, i.e. r_c ($0 < r_c < r_s$). So we replace $\int f(r)dr$ by $1/2f(r_c)\Delta_r$ where Δ_r is the interval of integration, and $f(r)$ is the function of comoving radial distance r under consideration. Similarly we replace the $\omega(r)$ dependence in the \mathbf{k} integrals by $\omega_{\text{SZ}}(r_c)$. Under these approximations we can write:

$$\Phi_{\tilde{\Theta}}(y) = \phi(y); \quad h_{\tilde{\Theta}}(x) = h(x) \quad (45)$$

Thus we find that the statistics of the underlying field $1+\delta$ and the statistics of the reduced field η are exactly the same under such an approximation (the approximate functions Φ_η and $h_\eta(x)$ do satisfy the proper normalization constraints). Although it is possible to integrate the exact expressions of the scaling functions, there is some uncertainty involved in the actual determination of these functions and associated parameters such as ω, k_a, x_* from N-body simulations (e.g. see Munshi et al. 1999, Valageas et al. 1999 and Colombi et al. 1996 for a detailed description of the effect of the finite volume correction involved in their estimation). We have used $\Phi_{\tilde{\Theta}}(y)$ as derived above to compute $P(\tilde{\Theta})$ with the help of Eq.(27).

An Edgeworth expansion of the pdf can be made by starting with the simpler form $P(\tilde{\Theta}(\theta_b))$, which can then be used to construct the Edgeworth series for $P(\Theta_{\text{SZ}}(\theta_b))$. The Edgeworth expansion (see e.g. Bernardeau & Koffman 1994) is meaningful when the variance is less than unity, which guarantees a convergent series expansion in terms of Hermite polynomials $H_n(\nu)$, of order n and with $\nu = \tilde{\Theta}/\sqrt{\langle \xi_{\tilde{\Theta}} \rangle}$. Hence it is used in quasi-linear analysis with the perturbative expressions for cumulants. However the $S_N^{\tilde{\Theta}}$ parameters used in the expansion of $P(\tilde{\Theta})$ are from the highly non-linear regime; i.e. although the variance is smaller than unity, the parameters that characterize it are from the highly non-linear dynamics of the underlying dark matter distribution.

$$p(\tilde{\Theta}) \equiv \frac{1}{\sqrt{2\pi\xi_{\tilde{\Theta}}}} \exp\left(-\frac{\nu^2}{2}\right) \left[1 + \sqrt{\xi_{\tilde{\Theta}}} \frac{S_3^{\tilde{\Theta}}}{6} H_3(\nu) + \sqrt{\xi_{\tilde{\Theta}}}^2 \left(\frac{S_4^{\tilde{\Theta}}}{24} H_4(\nu) + \frac{S_3^{\tilde{\Theta}2}}{72} H_6(\nu) \right) + \dots \right] \quad (46)$$

So we can express the relations connecting the probability distribution function for the smoothed statistics of $\Theta_{\text{SZ}}(\theta_b)$, the reduced field $\eta(\theta_b)$, i.e. we can write $P(\Theta_{\text{SZ}}(\theta_b)) = P(\tilde{\Theta})/\tilde{\Theta}_{\text{SZ}}$. Throughout our analysis we have used a Gaussian beam for smoothing the y maps, but our study can be extended to other windows too. The formalism which we have developed for one-point statistics such as the PDF and the VPF can also be extended to compute the bias and higher order cumulants associated with spots in y maps above a certain threshold. The statistics of such spots can be associated with the statistics of over-dense regions in the underlying mass distribution which represent the collapsed objects. A detailed analysis of these issues was presented in Munshi & Coles (1999b).

In addition to the generating function approach we have used the lognormal distribution to model the underlying distribution (see Appendix-A for a detailed discussion on the lognormal distribution). In Figure-(2) we have presented the results of our calculations for the entire range of smoothing angular scales. In Figure-(3) we have displayed the result of numerical computation for the PDF for various beam sizes as indicated.

6.1 The bias associated with the SZ sky

To compute the bias associated with the peaks in the SZ field we have to first develop an analytic expression for the generating field $\beta_{\tilde{\Theta}}(y_1, y_2)$ for the SZ field $\tilde{\Theta}^{\text{SZ}}(\theta_0) = \Theta^{\text{SZ}}(\theta_0)/\tilde{\Theta}^{\text{SZ}}(\theta_0)$. For that we will use the usual definition for the two-point cumulant correlator $C_{pq}^{\tilde{\Theta}}$ for the field; for a complete treatment of statistical properties of Θ_s see Munshi & Coles (1999b).

$$C_{pq}^{\tilde{\Theta}} = \frac{\langle \tilde{\Theta}_{\text{SZ}}(\hat{\Omega}_1)^p \tilde{\Theta}_{\text{SZ}}(\hat{\Omega}_2)^q \rangle}{\langle \tilde{\Theta}_{\text{SZ}}^2(\theta_b) \rangle^{p+q-2} \langle \tilde{\Theta}_{\tilde{\Theta}}(\hat{\Omega}_1) \tilde{\Theta}_{\tilde{\Theta}}(\hat{\Omega}_2) \rangle} = C_{p1}^{\tilde{\Theta}} C_{q1}^{\tilde{\Theta}} \quad (47)$$

We will show that, as is the case with its density field counterpart the two-point generating function for the field Θ_{SZ} can also be expressed (under certain simplifying assumptions) as a product of two one-point generating functions $\beta^{\text{SZ}}(y)$ which can then be directly related to the bias associated with ‘‘hot-spots’’ in y -maps.

$$\beta_{\bar{\Theta}}(y_1, y_2) = \sum_{p,q} \frac{C_{pq}^{\bar{\Theta}}}{p!q!} y_1^p y_2^q = \sum_p \frac{C_{p1}^{\bar{\Theta}}}{p!} y_1^p \sum_q \frac{C_{q1}^{\bar{\Theta}}}{q!} y_2^q = \beta_{\bar{\Theta}}(y_1) \beta_{\bar{\Theta}}(y_2) \equiv \tau_{\bar{\Theta}}(y_1) \tau_{\bar{\Theta}}(y_2) \quad (48)$$

It is clear that the factorization of generating function actually depends on the factorization property of the cumulant correlators i.e. $C_{pq}^{\bar{\Theta}} = C_{p1}^{\bar{\Theta}} C_{q1}^{\bar{\Theta}}$. Note that such a factorization is possible when the correlation of two patches in the directions $\hat{\Omega}_1$ and $\hat{\Omega}_2$ $\langle \Theta_{\text{SZ}}(\hat{\Omega}_1) \Theta_{\text{SZ}}(\hat{\Omega}_2) \rangle_c$ is smaller compared to the variance $\langle \Theta_{\text{SZ}}^2(\theta_b) \rangle$ for the smoothed patches

$$\beta_{\bar{\Theta}}(y_1, y_2) = \sum_{p,q} \frac{1}{p!q!} \frac{y_1^p y_2^q}{\langle \bar{\Theta}_{\bar{\Theta}}^2(\theta_b) \rangle^{p+q-2}} \frac{\langle \bar{\Theta}_{\text{SZ}}(\hat{\Omega}_1)^p \bar{\Theta}_{\text{SZ}}(\hat{\Omega}_2)^q \rangle}{\langle \bar{\Theta}_{\text{SZ}}(\hat{\Omega}_1) \bar{\Theta}_{\text{SZ}}(\hat{\Omega}_2) \rangle}. \quad (49)$$

We will now use the integral expression for the cumulant correlators (Munshi & Coles 1999a) in order to express the generating function which, in turn, uses the hierarchical *ansatz* and the far-field approximation as explained above

$$\beta_{\bar{\Theta}}(y_1, y_2) = \sum_{p,q} \frac{C_{pq}^{\text{SZ}}}{p!q!} \frac{y_1^p}{\langle \bar{\Theta}_{\text{SZ}}^2(\theta_b) \rangle^{p-1}} \frac{y_2^q}{\langle \bar{\Theta}_{\text{SZ}}^2(\theta_b) \rangle^{q-1}} \frac{1}{\xi_{\text{SZ}}^{12}} \int_0^{r_s} dr d_A^2(r) b_{\pi}^{p+q}(r) \frac{\omega_{\text{SZ}}^p(r) \omega_{\text{SZ}}^q(r)}{d_A(r)^{2p} d_A(r)^{2q}} [\mathcal{I}_{\theta_0}]^{p+q-1} \mathcal{I}_{\theta_{12}} \quad (50)$$

It is possible to further simplify the above expression by separating the summation over dummy variables p and q , which will be useful to establish the factorization property of two-point generating function for bias $\beta_{\bar{\Theta}}(y_1, y_2)$. We can now decompose the double sum over the two indices into two separate sums over individual indices. The above expression is quite general and depends only on the small angle approximation and the large separation approximation and is valid for any given specific model for the generating function $\mathcal{G}(\tau)$. However it is easy to notice that the projection effects as encoded in the line of sight integration do not allow us to write down the two-point generating function $\beta_{\bar{\Theta}}(y_1, y_2)$ simply as a product of two one-point generating functions $\beta_{\bar{\Theta}}(y)$ as was the case for the density field $1 + \delta$. As in the case of the derivation of the probability distribution function for the smoothed field Θ_{SZ} it now simplifies matters if we define a reduced smoothed tSZ field η_s . The statistical properties of η_s are very similar to that of the underlying 3D density field (under certain simplifying approximations) and are roughly independent of the background geometry and dynamics of the universe,

$$\beta_{\bar{\Theta}}(y_1, y_2) = \int_0^{r_s} dr \frac{w_{\text{SZ}}(r)}{\bar{\Theta}_{\text{SZ}}} \frac{w_{\text{SZ}}(r)}{\bar{\Theta}_{\text{SZ}}} d_A^2(r) \frac{I_{\theta_{12}}}{\xi_{\text{SZ}}^{12}} \frac{\langle \Theta_s^2 \rangle}{I_{\theta_0}} \beta_{\text{SZ}} \left(b_{\pi}(r) \bar{\Theta}_{\text{SZ}} \frac{y_1}{\langle \Theta_s^2 \rangle} \frac{\omega_{\text{SZ}}(r)}{d_A^2(r)} \mathcal{I}_{\theta_0} \right) \frac{\langle \Theta_{\text{SZ}}^2(\theta_b) \rangle}{\mathcal{I}_{\theta_0}} \beta_{\text{SZ}} \left(b_{\pi}(r) \bar{\Theta}_{\text{SZ}} \frac{y_2}{\langle \Theta_{\text{SZ}}^2(\theta_b) \rangle} \frac{\omega_{\text{SZ}}(r)}{d_A^2(r)} \mathcal{I}_{\theta_0} \right). \quad (51)$$

While the above expression is indeed very accurate and relates the generating function of the density field with that of the tSZ field, it is difficult to handle for any practical purpose. Also it is important to notice that the scaling functions such as $h(x)$ for the density probability distribution function and $b(x)$ for the bias associated with overdense objects are typically estimated from numerical simulations specially in the highly non-linear regime. Such estimations are plagued with several uncertainties such as finite size of the simulation box. It was noted in earlier studies that such uncertainties lead to only a rather approximate estimation of $h(x)$. The estimation of the scaling function associated with the bias i.e. $b(x)$ is even more complicated due to the fact that the two-point quantities such as the cumulant correlators and the bias are more affected by finite size of the catalogs. So it is not fruitful to actually integrate the exact integral expression we have derived above and we will replace all line of sight integrals with its approximate values. A study by Munshi & Jain (1999) used an exactly similar approximation to simplify the one-point probability distribution function for κ_s and found good agreement with ray tracing simulations. We will show that our approximation reproduces the numerical results quite accurately for a wide range of smoothing angle,

$$\bar{\Theta}_{\text{SZ}}(\theta_b) \approx \frac{1}{2} r_s b_{\pi}(r_c) (\omega_{\text{SZ}}(r_c)), \quad \langle \Theta_{\text{SZ}}^2(\theta_b) \rangle \approx \frac{1}{2} r_s \omega_{\text{SZ}}^2(r_c) b_{\pi}^2(r_c) \left[\frac{d^2 k}{(2\pi)^2} P_{\delta}(k) W^2(k d_A(r_c) \theta_b) \right], \quad (52)$$

$$\langle \Theta_{\text{SZ}}(\hat{\Omega}_1) \Theta_{\text{SZ}}(\hat{\Omega}_2) \rangle_c \approx \frac{1}{2} r_s \omega_{\text{SZ}}^2(r_c) b_{\pi}^2(r_c) \left[\frac{d^2 k}{(2\pi)^2} P_{\delta}(k) W^2(k d_A(r_c) \theta_b) \exp[ik d_A(r_c) \theta_{12}] \right]. \quad (53)$$

Use of these approximations gives us the leading order contributions to these integrals and we can check that to this order we recover the factorization property of the generating function i.e. $\beta_{\bar{\Theta}}(y_1, y_2) = \beta_{\eta}(y_1) \beta_{\eta}(y_2) = \beta_{1+\delta}(y_1) \beta_{1+\delta}(y_2) \equiv \tau(y_1) \tau(y_2)$. So it is clear that at this level of approximation, due to the factorization property of the cumulant correlators, the bias function $b_{\eta}(x)$ associated with the peaks in the field Θ_{SZ} , beyond certain threshold, obeys a similar factorization property too, which is exactly same as its density field counterpart. Earlier studies have established such a correspondence between the tSZ field and density field in the case of one-point probability distribution function $p(\delta)$ (Munshi & Jain 1999b),

$$b_{\bar{\Theta}}(x_1) h_{\bar{\Theta}}(x_1) b_{\bar{\Theta}}(x_2) h_{\bar{\Theta}}(x_2) = b(x_1) h(x_1) b(x_2) h(x_2). \quad (54)$$

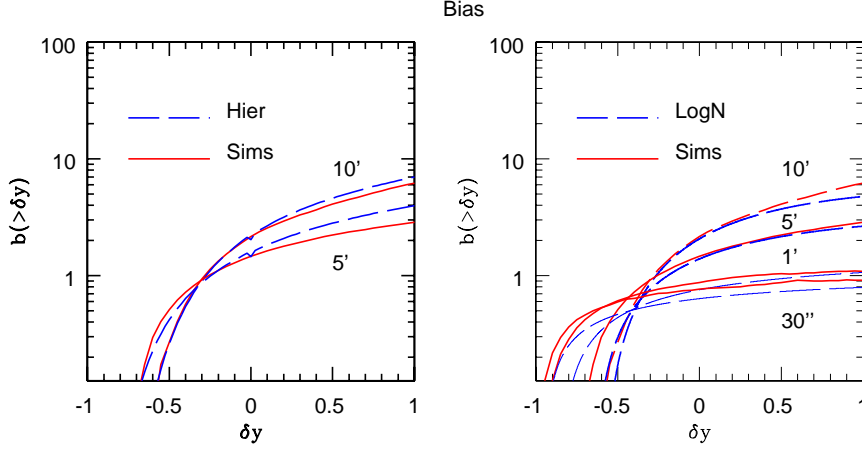


Figure 4. The cumulative bias associated with $b(> \delta y)$ is plotted as a function of δy . Various curves correspond to different beam size (FWHM) as indicated. Two different analytical models are shown; the lognormal (right-panel) and the hierarchical ansatz (left-panel). The solid lines correspond to the results from numerical simulations. The dashed lines in each panel represent the analytical results.

Where we have used the following relation between $\beta_\eta(y)$ and $b_\eta(x)$,

$$b_{\bar{\Theta}}(x)h_\eta(x) = -\frac{1}{2\pi i} \int_{-i\infty}^{i\infty} dy \tau(y) \exp(xy). \quad (55)$$

For all practical purpose we found that the differential bias as defined above is more difficult to measure from numerical simulations as compared to its integral counterpart where we concentrate on the bias associated with peaks above certain threshold,

$$b_{\bar{\Theta}}(> x)h_{\bar{\Theta}}(> x) = -\frac{1}{2\pi i} \int_{-i\infty}^{i\infty} dy \frac{\tau(y)}{y} \exp(xy). \quad (56)$$

It is important to notice that although the bias $b(x)$ associated with the SZ field Θ_{SZ} and the underlying density field is exactly same, the variance associated with the density field is very high but the projection effects in the tSZ field brings down the variance to a value less than unity which indicates that we have to use the integral definition of bias to recover it from its generating function (see eq.(55) and eq.(56)). Now writing down the full two point probability distribution function for two correlated spots in terms of the SZ field $\Theta_{\text{SZ}}(\theta_b)$ and its reduced version $\bar{\Theta}$:

$$p_{\text{SZ}}(\Theta_{\text{SZ}}^{(1)}, \Theta_{\text{SZ}}^{(2)})d\Theta_{\text{SZ}}^{(1)}d\Theta_{\text{SZ}}^{(2)} = p_{\text{SZ}}(\Theta_{\text{SZ}}^{(1)})p_{\text{SZ}}(\Theta_{\text{SZ}}^{(2)})(1 + b_{\text{SZ}}(\Theta_{\text{SZ}}^{(1)})\xi_{12}^{\text{SZ}}b_{\text{SZ}}(\Theta_{\text{SZ}}^{(2)}))d\Theta_{\text{SZ}}^{(1)}d\Theta_{\text{SZ}}^{(2)}, \quad (57)$$

$$p(\bar{\Theta}_1, \bar{\Theta}_2)d\bar{\Theta}_1d\bar{\Theta}_2 = p(\bar{\Theta}_1)p(\bar{\Theta}_2)(1 + b(\bar{\Theta}_1)\tilde{\xi}_{12}b(\bar{\Theta}_2))d\bar{\Theta}_1d\bar{\Theta}_2 \quad (58)$$

In our analysis of pdf we found that $p_{\text{SZ}}(\Theta) = p_{\bar{\Theta}}(\bar{\Theta})/\bar{\Theta}$ we also noticed that $\tilde{\xi}_{12} = \xi_{12}^{\text{SZ}}/[\bar{\Theta}]^2$. Using these relations we can now write: $b_{\text{SZ}}(\Theta) = b(\bar{\Theta})/\bar{\Theta}$. The results derived here can be generalized to cross-correlation analysis and will be presented elsewhere. It is important to realize that the bias $b_{\text{SZ}}(\Theta)$ is related to the bias of “hot-spots” in the tSZ-map and relates their distribution with the overall correlation structure of the tSZ-maps. The bias defined earlier b_π on the other hand relates the 3D pressure distribution $\pi(\mathbf{x})$ and the underlying density distribution $\delta(\mathbf{x})$.

In Figure-4 we have shown the integrated bias $b(> \delta y)$ computed using two different analytical techniques as function of the threshold δy . In the right panel the various smoothing angular scales FWHM we have shown correspond to $\theta_b = 30'', 1', 5', 10'$. The solid lines correspond to the numerical simulations. The dashed lines correspond to predictions from the lognormal model. This bias for higher δy regions is higher. The results for the perturbative calculations are shown only for $\theta_b = 10', 5'$. For smaller beam the perturbative calculations break down.

7 CONCLUSIONS

We have studied the prospects of extracting the non-Gaussian statistical signatures from ongoing and future CMB surveys. The tSZ effect is associated with the hot-gas in large-scale structure that is being probed by the multi-frequency experiments such as Planck. When compared with the CMB temperature anisotropies, the tSZ effect has a distinct spectral dependence with a null at a frequency of 217 GHz. This distinct spectral

signature of SZ effect means it can be effectively separated from the primary CMB contributions. This will provide an unique opportunity to probe tSZ effect using data from ongoing survey such as Planck. The statistical analysis of frequency separated SZ maps has so far been mainly focused on lower order statistics. Non-Gaussianity in the tSZ signal is an additional information that is useful in constraining the large scale pressure fluctuation associated with the tSZ effect. This signature can be useful for the detection and characterization of the tSZ effect as well for separating it from other secondaries.

The tSZ effect traces the pressure fluctuations associated with large scale distribution of the baryonic gas. The generation of pressure fluctuation in the virialized dark matter halos can be modeled by assuming them to be in hydrostatic equilibrium with the dark matter distribution in the halo. The presence of shock-heated gas typically corresponds to overdensities in excess of $\delta \geq 200$. The unshocked, photoionized baryonic gas typically traces the large scale distribution of dark matter distribution. The typical overdensity corresponding to the presence of unshocked photoionised baryons is less than $\delta \leq 10$.

We have modeled the tSZ effect using a simplistic biasing model that rely on a perturbative description of dark matter clustering. The statistics of the hot-gas is linked to that of the dark matter using a redshift dependent biasing scheme. While this type of modeling is adequate for small overdensities a more elaborate analytical scheme is required for detailed description of baryonic clustering at smaller scales. We construct the entire cumulant generating function and show that under certain simplification it becomes independent of the details of the biasing scheme. The generating function adopted here was developed primarily for the construction of 3D and 2D (projected) density distribution that are studied using galaxy surveys. Later it was used in construction of weak lensing PDF in small and large smoothing angular scales. In this paper we have shown that a similar technique can be adopted for the study of tSZ when it is expressed in terms of the 3D pressure fluctuations. We have compared these results against simulations. In the angular scales where the rms fluctuation in δy maps is smaller than unity hence the perturbative series is valid and the analytical predictions are in very good agreement with numerical simulations. We find our analytical results to be accurate for the angular scales larger than few arc-minutes ($\theta_b > 2'$). As a result of our study we notice that even at a comparatively large angular scales $\theta_b > 10'$ the PDF distribution of the tSZ effect is highly non-Gaussian. While the tSZ power spectrum is sensitive to the amplitude of the density fluctuations σ_8 the higher order statistics such as skewness of the tSZ effect can be used to separate out the pressure bias from the amplitude of the density fluctuations.

In addition to the perturbative approach or the hierarchical *ansatz* we have also used a model based on the lognormal distribution. The lognormal model is non-perturbative and have been used widely in the literature. Like the perturbative approach it has been used to model the results from galaxy surveys (Hamilton 1985; Coles & Jones 1991; Bouchet et al 1993; Kofman et al. 1994), weak lensing observables (Munshi 2000; Taruya et al. 2002) as well as Lyman-alpha statistics (Bi & Davidson 1997). The validity of the lognormal model has been compared against numerical simulations as well as against the perturbative or hierarchical methods (Bernardeau & Kofman 1995).

In the entire range of angular scales studied by us we find the lognormal model to be a very good approximation for the scaled δy parameter distribution. We have also checked that the mean μ and the variance Σ of the lognormal distribution satisfies the constraint $2\mu = -\Sigma$ for most of the range of scales probed by us. This is a necessary condition for the validity of any modeling based on the direct linear biasing considered in the perturbative approach. The validity of the lognormal model thus supports the results from the linear biasing scheme. It means that the statistics of δy which is a projected quantity is equivalent to the 3D density contrast δ ; a result that was obtained also using perturbative approach Eq.(45). Thus Eq.(A7) is a major consistency check beyond order by order calculation of the the perturbative approach. Ofcourse the validity of the lognormal approximation also means validity of such an approximation go beyond the validity range of the perturbative approach. The perturbative approach was used for the construction of both one-point and the two-point PDFs. In a similar way the bivariate lognormal distribution too was used to model the biivariate distribution of the δy parameter.

Many previous studies have considered a halo model based approach for modeling the distribution of the gas in collapsed virialised halos in which the specific number density and the radial profile of these halos are analysed using Press-Sechter formalism or its variants. However detailed modeling of the complete PDF or bias associated with the spots of high δy is possible in this approach only in an order by order manner. In our perturbative or lognormal based analysis we go the beyond order by order approach and construct the entire cumulant generating function $\Phi(y)$ and relate it to that of the underlying density distribution $\phi(y)$. This allows us to reproduce and predict the entire PDF of the tSZ distribution for a specific smoothing angular scale. The statistical picture that we have developed here is complementary to the one based on PS based approach.

Few comments on the validity of the perturbative results are in order. The tSZ power spectrum by and large depends on the one halo term in the halo modeling. However in the perturbative regime we are mostly probing gas as if it were coarsely grained on the Jeans scale, i.e. that part which is not in collapsed objects and traces the smoothed large scale dark matter distribution. While analysing the tZ maps it is expected that removal of X-ray bright clusters can reduce contributions from collapsed halos. The effect captured by the linear biasing should be understood as a signal in blank fields where such clusters are not present. It provides the lower limit of tSZ effect from large scale structure distribution.

We would like to point out that previous studies have modelled the statistics of tSZ effect using hierarchical ansatz (Valageas & Silk 1999; Valageas, Schaeffer & Silk 2002). However in such studies the contribution from individual halos were computed using a virialization scheme and equilibrium profile for the pressure distribution within the halos. The results presented here are complementary to such results as we focus on large-scale distribution of hot gas. In stead of modeling contribution from individual halos we directly link the baryonic pressure fluctuation responsible for large scale tSZ effect in terms of the underlying mass distribution.

The method that we pursue here depends on frequency cleaned tSZ maps. The tSZ effect can also be studied using cross-correlation techniques that involve external tracers. Such methods typically employ mixed bispectrum. The results however lack the frequency information and typically

confusion noise dominated from It is possible to study tSZ effect using mixed bispectrum use of frequency cleaned maps typically provide additional signal-to-noise due to the frequency information. In the absence of frequency information the background CMB plays the role of intrinsic noise that degrades the signal-to-noise ratio. It is also interesting to note that removal of tSZ from the CMB maps may actually help in detection of other sub-dominant effects.

In some sense observations of the Lyman alpha statistics which probes the large scale distribution of cold neutral gas is complementary to tSZ studies of hot ionized gas. The formalism developed here will also be useful for analysing the statistics of other secondaries in CMB. Results of such analyses will be presented elsewhere.

8 ACKNOWLEDGEMENTS

DM acknowledges support from STFC standard grant ST/G002231/1 at School of Physics and Astronomy at Cardiff University where this work was completed. We would like to thank Alan Heavens, Patrick Valageas, Ludo van Waerbeke and Martin White for many useful discussions. We would like to thank Martin White for making his tSZ simulations data freely available which we have used in this work. We would also like to thank Francis Bernardeau for making a copy of his code available to us which we have modified to compute the PDF and bias of the tSZ field for the perturbative model. SJ and JS acknowledge support from from the US Department of Education through GAANN fellowships at UCI.

REFERENCES

- Aghanim N, Majumdar S., Silk J., 2008, Rept.Prog.Phys., 71, 066902
 Balian, R., Schaeffer, 1989, A&A, 220, 1
 Bernardeau F., Colombi S., Gaztanaga E., Scoccimarro R., 2002, Phys.Rept., 367, 1
 Bernardeau F., Schaeffer R., 1992, A&A, 255, 1
 Bernardeau F., Schaeffer R., 1999, A&A, 349 697
 Bernardeau, F., Kofman, L. 1995, ApJ, 443, 479
 Bernardeau, F. 1992, ApJ, 392, 1
 Bernardeau, F. 1994, A&A, 291, 697
 Birkinshaw M. 1999, Phys.Rep, 310, 98
 Bouchet, F., Strauss, M. A., Davis, M., Fisher, K. B., Yahil, A., Huchra, J. P. 1993, ApJ, 417, 36
 Bouchet F.R., Gispert R., 1999, New Astronomy, 4, 443
 Bi H. G. & Davidson A.F. 1997, ApJ, 479, 523
 Cao L., Liu J., Fang L.-Z. 2007, ApJ, 661, 641
 Cen R., Ostriker J.P., 1999, ApJ, 514, 1
 Coles P., Jones B. 1991, MNRAS, 248, 1
 Coles P., Melott A., Munshi D., 1999, ApJ, 521, 5
 Colombi S., 1994, ApJ, 435, L536
 Colombi S., Bouchet F.R., Hernquist L., 1996, ApJ, 465, 14
 Cooray A., Hu W. 2001, ApJ, 548, 7
 Cooray A., Hu W. & Tegmark M., 2000, ApJ, 540, 1
 Cooray A, 2000, PRD, 62, 103506
 Cooray A, 2001, PRD, 64, 063514
 Cooray A., 2001, PhRvD, 64, 043516
 Cooray A., Seth R., 2002, Phys. Rep. 372, 1
 Delabrouille J., Cardoso J., Patanchon G., 2003, MNRAS, 330, 807
 Goldberg, D.M. Spergel D.N., 1999, PRD, 59, 103001
 Goldberg, D.M. Spergel D.N., 1999, PRD, 59, 103002
 Hadwiger H. 1959, Normale Koper im Euclidschen raum und ihre topologischen and metrischen Eigenschaften, Math Z., 71, 124
 Hallman E.J., O'Shea B.W., Smith B.D., Burns J.O., Norman M.L. 2009, ApJ, 698, 1759
 Hallman E.J., O'Shea B.W., Burns J.O., Norman M.L., Harkness R., Wagner R., 2007, ApJ, 671, 27
 Hamilton, A. J. S. 1985, ApJ, 292, L35
 Hansen F., Branchini E., Mazzotta P., Cabella P., Dolag K., 2005, MNRAS, 361, 753
 Hivon E., Górski K. M., Netterfield C. B., Crill B. P., Prunet S., Hansen F., 2002, ApJ, 567, 2
 Hikage C., Coles P., Grossi M., Moscardini L., Dolag K., Branchini L., Matarrese S. 2008, MNRAS, 385, 1513

- Hikage C., Komatsu E., Matsubara T., 2006, *ApJ*, 653, 11
 Hikage C., Taruya A., Suto Y., 2003, *Publ.Astron.Soc.Jap*, 55, 335
 Hikage C., et al. *Publ.Astron.Soc.Jap*. 54 (2002) 707
 Hikage C., et al. *Publ.Astron.Soc.Jap*. 55 (2003) 911
 Hui L., 1999, *ApJ*, 519, L9-12
 Joudaki S., Smidt J., Amblard A., Cooray A., 2010, *JCAP*, 1008, 027
 Kayo I., Taruya A., Suto Y. 2001, *ApJ*, 561, 22
 Komatsu E., Seljak U. 2002, *MNRAS*, 336,1256
 Kofman, L., Bertschinger, E., Gelb, J. M., Nusser, A., Dekel, A. 1994, *ApJ*, 420, 44
 Leach S.M., et al., *A&A*,491,597,2008
 Limber D.N., 1954, *ApJ*, 119, 665
 Lin K.-Y, Woo T.-P., Tseng Y.-H., Lin L., Chiueh T. 2004, *ApJ*, 608, L1
 LoVerde M., Afshordi N. 2008, *Phys.Rev.D*78, 123506
 Matarrese S., Lucchin F, Moscardini L, Saez D., 1992, *MNRAS*, 259, 437
 Mo H.J., White S.D.M. *MNRAS*, 1996, 282, 347
 Munshi D., Heavens A., 2010, *MNRAS*, 401, 2406
 Munshi D., Jain B., 2001,*MNRAS*, 322, 107
 Munshi D. Jain B., 2000, *MNRAS*, 318, 109
 Munshi D., 2000, *MNRAS*, 318, 145
 Munshi D., Coles P., 2000, *MNRAS*, 313, 148
 Munshi D., Coles P. Melott A., 1999, *MNRAS*, 310, 892
 Munshi D., Coles P. Melott A., 1999, *MNRAS*,307, 387
 Munshi D., Melott A., Coles P., 2000, *MNRAS*,311,149
 Munshi D., Sahni V., Starobinsky A., 1994, *ApJ*, 436, 517
 Navarro J., Frenk C., White S.D.M 1996, *ApJ*, 462, 563
 Peebles P.J.E., 1971, *Physical cosmology*, Princeton Series in Physics.
 Persi F., Spergel D. cen R., Ostriker J., 1995, *ApJ*, 442,1
 Press & Sechter 1974, *Astrophys.J*, 187, 425
 The Planck Collaboration, 2006, *astro-ph/0604069*
 Rephaeli Y. 1995, *ARA&A*, 33, 541
 Refregier A., Komatsu E., Spergel D.N., Pen U.-L., 2000, *PRD*, 61, 123001
 Runyan M.C. et al. 2003 *ApJS* 149 265
 Seljak U., Burwell J., Pen U.-L. 2001, *Phys.Rev. D*63, 063001
 Sunyaev R.A., Zeldovich Ya B., 1980, *ARA&A*, 18, 537
 Sunyaev R.A., Zeldovich Ya B., *Comments Astrophys. Space Phys*, 4, 173
 Scoccimarro, R.; Frieman, J. A., 1999, *ApJ*, 520, 35S
 Scoccimarro R., Couchman H.M.P., 2001,*MNRAS*, 325, 1312
 da Silva et al., Barbosa A.C., Liddle A.R., Thomas P.A., 1999, *MNRAS*
 Smidt J., Joudaki S., Serra P., Amblard A., Cooray A., 2010, *PRD*, 81, 123528
 Refregier A., Teyssier R., 2002, *PhRvD*, 66, 043002
 Roncarelli M., Moscardini L., Borgano S., Dolag K., 2007, *MNRAS*, 378, 1259
 Seljak U., *MNRAS*, 2000, 318, 203
 Springel V., White M. & Hernquist L., 2001, *ApJ*, 549,681
 Szapudi I., Colombi S., 1996, *ApJ*, 470, 131
 Szapudi I., Szalay A.S., 1993, *ApJ*, 408, 43
 Szapudi I., Szalay A.S., 1997, *ApJ*, 481, L1
 Szapudi I., Szalay A.S., Boschan P., 1992, *ApJ*, 390, 350
 Taruya A.,Takada M.,Hamana T., Futamase T., 2002, *ApJ*, 571, 638
 Taruya A., Takada M., Hamana T., Kayo I., Futamase T., 2002, *ApJ*, 571, 638
 Valageas P., Schaeffer R., Silk J., 2002, *A&A*, 388, 741
 Valageas P., Silk J., 1999, *A&A*, 347, 1
 Valageas P, Lacey C., Schaeffer R., 2000, *MNRAS*,311, 234
 White M., *ApJ*, 2003, 597, 650, 658
 White M., Hernquist V. & Springel V., 2002, *ApJ*, 579,16

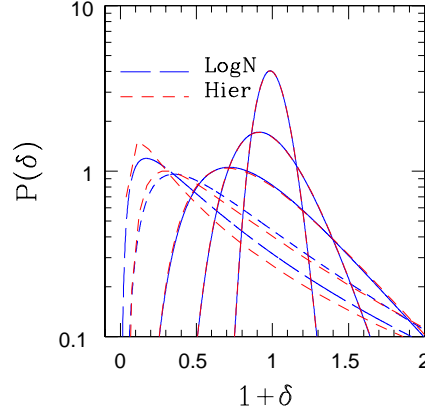


Figure A1. The PDF $p(\delta)$ as a function $1 + \delta$ for various values $\sigma = 0.1, 0.25, 0.5, 1.0, 1.5$. Two different approximations are considered, the lognormal (long dashed) and the hierarchical ansatz (short dashed). The broader PDFs correspond to higher values of σ . The lognormal distribution is computed using Eq.(A1) and Eq.(A2). The hierarchical ansatz based PDF is computed by direct contour integration involving the moment generating function using Eq.(27).

White S.D.M., 1979, MNRAS, 186, 145
 Zhang P., Pen U.-L., 2001, ApJ, 549, 18
 Zhang P., Pen U.-L., Trac H., 2004, MNRAS, 355, 451
 Zhang P., Seth R.K., 2007, ApJ, 579, 16

APPENDIX A: THE LOG-NORMAL DISTRIBUTION

The evolution of PDF of the density field δ is of primary interest in cosmology. It has been investigated in great detail in the past. In addition to the hierarchical ansatz that we have studied here there have been studies involving other distributions such as the negative binomial distribution or the log-normal distribution. Indeed log-normal distribution (also known as Galton distribution) has long been known as a successful empirical prescription for the characterization of the dark matter distribution as well as the observed galaxy distribution (Hamilton 1985; Coles & Jones 1991; Bouchet et al 1993; Kofman et al. 1994). Detailed discussion for comparison of lognormal distribution and the perturbative calculations can be found in (Bernardeau & Kofman 1995). The lognormal distribution was further generalised to the *skewed*-lognormal distribution (Colombi 1994). In general a variable might be modeled as lognormal if it can be thought of as the multiplicative product of many independent random variables.

Although inherently local in nature the lognormal distribution can provide a good fit to both one-point PDF and its generalisation to compute its two-point analog and hence the bias (Taruya et al. 2002). The one- and two-point lognormal pdf can be expressed as (Kayo, Taruya, Suto 2001):

$$p(\delta)d\delta = \frac{1}{\sqrt{2\pi\Sigma^2}} \exp\left[-\frac{\Lambda^2}{2\Sigma^2}\right] \frac{d\delta}{1+\delta}; \quad (\text{A1})$$

$$\Sigma = \ln(1 + \sigma^2); \quad \Lambda = \ln[(1 + \delta)\sqrt{(1 + \sigma^2)}]; \quad (\text{A2})$$

$$p(\delta_1, \delta_2)d\delta_1d\delta_2 = \frac{1}{2\pi\sqrt{\Sigma^2 - X_{12}^2}} \exp\left[-\frac{\Sigma(\Lambda_1^2 + \Lambda_2^2) - 2X_{12}\Lambda_1\Lambda_2}{2(\Sigma^2 - X_{12}^2)}\right] \frac{d\delta_1}{1+\delta_1} \frac{d\delta_2}{1+\delta_2}; \quad (\text{A3})$$

$$\Lambda_i = \ln[(1 + \delta_i)\sqrt{(1 + \sigma^2)}]; \quad X_{12} = \ln(1 + \xi_{12}) \quad (\text{A4})$$

In the limiting case of large separation $X_{12} \rightarrow 0$ we can write down the two point PDF

$$p(\delta_1, \delta_2) = p(\delta_1)p(\delta_2)[1 + b(\delta_1)\xi_{12}b(\delta_2)]; \quad b(\delta_i) = \Lambda_i/\Sigma. \quad (\text{A5})$$

It is however easier to estimate the cumulative or integrated bias associated with objects beyond a certain density threshold δ_0 . This is defined as $b(\delta > \delta_0) = \int_{\delta_0}^{\infty} p(\delta)b(\delta)d\delta / \int_{\delta_0}^{\infty} p(\delta)d\delta$. In the low variance limit $\sigma^2 \rightarrow 0$ the usual Gaussian result is restored $b(\delta) = \delta/\sigma^2$. The parameters $\Lambda, \Lambda_i, X_{12}, \Sigma$ that we have introduced above can be expressed in terms of the two-point (non-linear) correlation function $\xi_{12} = \langle \delta_1\delta_2 \rangle$ and the

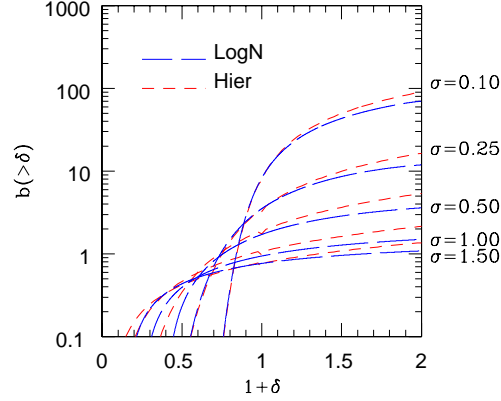


Figure A2. The bias $b(> \delta)$ as a function $1 + \delta$ for various values $\sigma = 0.1, 0.25, 0.5, 1.0, 1.5$. Two different approximations are considered, the lognormal distribution (long dashed) and the hierarchical ansatz (short dashed). The analytical results in each case correspond to for large separation approximation. The bias according to the lognormal model is defined in Eq.(A3) and Eq.(A4). The hierarchical ansatz based bias is computed using Eq.(27) which involves direct contour integration in the complex plane.

nonlinear variance $\sigma^2 = \langle \delta^2 \rangle$ of the smoothed density field. To understand the construction of lognormal distribution, we introduce a Gaussian PDF in variable x $p(x) = (2\pi\Sigma^2)^{1/2} \exp[-(x - \mu)^2/2\Sigma^2]$. With a change of variable $x = \ln(y)$ we can write down the PDF of y which is a lognormal distribution $p(y) = (2\pi\Sigma^2)^{1/2} \exp[-(\ln(y) - \mu)^2/2\Sigma^2]/y$. The extra factor of $(1/x)$ stems from the fact: $dy/y = dx$. Note that y is positive definite and is often associate with $\rho/\rho_0 = 1 + \delta$ which means $\langle y \rangle = 1$. The moment generating function for the lognormal interms of the mean μ and the variance Σ has the following form:

$$\langle y^n \rangle = \exp(n\mu + n^2\Sigma^2/2). \quad (\text{A6})$$

This however leads to the fact that if the underlying distribution of x or the density is Gaussian we will have to impose the condition:

$$\mu = -\Sigma^2/2. \quad (\text{A7})$$

Here in our notation above Σ is the distribution of the underlying Gaussian field. The variance of y defined as $\langle y^2 \rangle - \langle y \rangle^2 = \exp(\Sigma^2) - 1 = \sigma^2$. So we can write $\Sigma^2 = \ln(1 + \sigma^2)$. This is the result that was used above. The generalisation to two-point or bivariate PDF can be done following the same arguments and can be found in (Kayo, Taruya, Suto 2001). The validity and limitations of the one-point and two-point PDFs have been studied extensively in the literature against N-body simulations. In Bernardeau (1992, 1994) it was shown that the PDF computed from the perturbation theory in a weakly nonlinear regime approaches the lognormal distribution function only when the primordial power spectrum is locally of the form $P(k) \propto k^{n_e}$ with the effective local spectra slope of the power spectrum $n_e \sim -1$. It was also shown that in the weakly nonlinear regime the lognormal distribution is equivalent to the hierarchical model with a generating function $\mathcal{G}(\tau) = \exp(-\tau)$. This leads to the skewness parameter $S_3 = 3 + \sigma^2$ and $S_4 = 16 + 15\sigma^2 + 6\sigma^4 + \sigma^6$. In general the $\sigma^2 \rightarrow 0$ leads to $S_p = p^{p-2}$. On this basis Bernardeau & Kofman (1995) argues that the agreement of lognormal PDF with numerical simulations should be interpreted as purely accidental and the success of the lognormal model is simply related to the fact that for all scales relevant to cosmology the CDM power spectrum can be approximated with a power law with effective slope $n_e \approx -1$. However subsequent studies using numerical simulation it was shown by various authors (see e.g. Kayo, Taruya, Suto (2001)) that the lognormal distribution very accurately describes the cosmological distribution functions even in the nonlinear regime $\sigma \leq 4$ for a relatively high values of density contrast $\delta < 100$. In Table-A1 we have presented the values of the variance Σ^2 as derived from the mean μ of the Gaussian PDF of $\log(y/\langle y \rangle)$ as well as from direct evaluation. We compare the variance σ^2 of $y/\langle y \rangle$ maps as well as estimates from Σ^2 . As can be seen that $\Sigma^2 = -2\mu$ is a fairly good approximation and $y/\langle y \rangle$ can be approximated reasonably well with a lognormal distribution for the range of angular scales probed.

Lognormal distribution has already been used to model the statistics of weak lensing observables (Munshi 2000; Taruya et al. 2002) and the clustering of Lyman alpha absorption systems (e.g. Bi & Davidson (1997)). One to one mapping of initial density fields to evolved density fields using maps that are consistent with lognormal distribution function was not found to be very successful and the success of lognormal distribution function in reproducing the statistics of gravitational clustering still remains somewhat unclear. However from our study in this paper it seems that lognormal distribution can be used very effectively to model the tSZ effect.

It is worth mentioning here that using a generating function approach in the quasi-linear regime (Munshi, Sahni, Starobinsky 1994) it was

Table A1. Mean and Variance of the Lognormal Distribution as a function of beam size

Beam	-2μ	Σ^2	σ^2	$\exp(\Sigma^2) - 1$
10'	0.19	0.17	0.18	0.18
5'	0.41	0.35	0.38	0.41
1'	1.49	1.35	2.42	2.84
30''	2.17	2.35	8.6	9.57

shown that well known *Frozen Flow* Approximation (Matarresse et al. 1992) that was proposed to extend the validity of Zeldovich Approximation beyond the formation of pancakes has exactly same generating function or the pdf as the log-normal distribution.